

A Counter-Current Gaseous Diffusion Model of Oxidation through a  
Porous Coating

G. R. Holcomb\*

\*Albany Research Center, U.S. Bureau of Mines, Albany, OR 97321.

## **ABSTRACT**

---

A counter-current gaseous diffusion model is presented to describe oxidation through porous coatings and scales. The specific system modeled is graphite oxidized through a porous alumina overcoat between 570 and 975°C. The model separates the porous alumina coating into two gas diffusion regions separated by a flame front, where O<sub>2</sub> and CO react to form CO<sub>2</sub>. In the outer region O<sub>2</sub> and CO<sub>2</sub> counter-diffuse; in the inner region CO<sub>2</sub> and CO counter-diffuse. The concentration gradients of each gaseous specie in the pores of the alumina are determined and the rate of oxidation is calculated. The model was verified by oxidation experiments of graphite through various porous alumina overcoats. The alumina overcoats ranged in porosity and in average pore radius from 0.077 μm (Knudsen diffusion) to 10.0 μm (molecular diffusion). The predicted and measured oxidation rates are shown to have the same dependence upon porosity, average pore radius, temperature and oxygen partial pressure. The use of the model is proposed for other oxidation systems and for chemical vapor infiltration. This work was part of the U. S. Bureau of Mines corrosion research program.

KEY WORDS: oxidation; gaseous diffusion; counter-current diffusion; carbon; graphite; alumina; porosity; chemical vapor infiltration.

## INTRODUCTION

---

Many materials, when oxidized, have both a solid and a gaseous oxidation product. The solid product can grow at the solid-gas interface with a porous structure, to allow the gaseous product to escape. In some cases, oxidation kinetics may be described by counter-current diffusion of oxygen inward and the gaseous product outward through the porous layer. This has been proposed as the oxidation mechanism of HfC between 1200 and 1530°C<sup>1-4</sup>.

An analogous situation may occur during oxidation of a material, such as carbon, through a porous coating; oxygen diffuses inward and CO/CO<sub>2</sub> diffuses outward. The oxidation kinetics and model of such a system, porous alumina coated graphite, is presented here as a simpler system (than HfC) to verify the gaseous counter-current diffusion model. Some of the complexities of the HfC system are absent: the porous scale is not growing (linear kinetics as opposed to parabolic), and the porosity of the scale is constant with respect to both time and to distance from the base material/porous material interface. Additionally, various porous alumina overcoats can be chosen in order to vary the porosity and pore size of the porous layer.

During oxidation of porous alumina coated graphite, CO gas is liberated at the graphite/alumina interface. The equilibrium constant between carbon, CO, and CO<sub>2</sub> is used to describe this reaction. Connected porosity allows for inward diffusion of O<sub>2</sub> gas and outward escape of CO gas. At elevated temperatures, CO

and  $O_2$  gas mixtures are not compatible and react to form  $CO_2$  gas. The  $CO_2$  reaction can occur within the porous alumina and, analogous to carbon oxidation without a coating, the position where it occurs may be termed a "flame front". The  $CO_2$  gas generated at the flame front diffuses both inward towards the graphite/alumina interface and outward towards the  $O_2$  atmosphere. An analysis of the counter-current diffusion of the  $CO/CO_2$  and  $O_2/CO_2$  gas mixtures, and the position of the flame front, form the basis of the counter-current gaseous diffusion model presented here.

A similar model was presented by Bernstein and Koger<sup>5</sup> for carbon film undercut kinetics in pure oxygen. The kinetics of a process was presented for fabricating micromechanical structures in which a sacrificial layer of carbon is deposited on a substrate, followed by a top layer of a different material. After oxidation of the carbon layer, the top layer is left free. One of the boundary conditions used was pure CO gas at the carbon interface, rather than using an equilibrium constant to relate the CO and  $CO_2$  partial pressures. Below  $700^\circ C$ , the measured oxidation rates were found to be slower than expected. It will be shown how the use of an equilibrium constant boundary condition, as opposed to a pure CO gas boundary condition, would result in the prediction of higher oxidation rates below  $700^\circ C$ .

## **EXPERIMENTAL**

---

Samples of graphite with porous alumina overcoats were constructed as shown in Fig. 1. The bottom section is the porous

alumina overcoat. The middle section is a disk of fine grained graphite inside a cored solid alumina square. The top is solid alumina. Alumina cement was used on all interior surfaces of the solid alumina, and along the outside edges. The solid alumina pieces were 99.8%-pure recrystallized alumina.

Five different porous aluminas were used for the overcoats: Coors<sup>†</sup> AP-998-C, P $\frac{1}{2}$ B-C, P-6-C, P-12-C, and P-40-C. These were selected to provide distinct differences in porosity and pore size. A mercury porosimeter was used to characterize the porous aluminas, as shown in Table 1.

The sample was suspended porous alumina side down by platinum wire in a 2" diameter reaction tube from a microbalance. A dry mixture of oxygen and nitrogen gas flowed up the reaction tube at a rate of 50 cm/min. The gas compositions ranged from 0.02 to 0.55 partial pressure of oxygen ( $P_{O_2}$ ). The reaction tube was within a vertical tube furnace. The temperature was controlled from a thermocouple placed just below the sample (within the reaction tube). Test temperatures ranged from 570 to 985 °C.

For each experiment, the sample was heated in dry nitrogen to 100°C above the test temperature and held there for one hour to insure that the alumina cement set completely. Then the temperature was lowered to the test temperature and after it stabilized, the dry oxygen/nitrogen mix was introduced into the chamber and the mass change was monitored. For each experiment, an initial low value of  $P_{O_2}$  (.023 to .044) was used and held constant for 15-30 minutes. Then the  $P_{O_2}$  was increased by steps

(and held constant for 15-30 minutes at each  $P_{O_2}$ ) until it reached a value of 0.50 to 0.55. Finally, the last measurements were made with the same  $P_{O_2}$  used initially. A comparison of the oxidation rates of the initial and final (at the same low  $P_{O_2}$ ) measurements served as a check against cracking or geometrical changes due to carbon loss that may have occurred during the experiment.

Because the alumina cement itself was porous, control samples using dense alumina for both the top and bottom of the specimen were oxidized. These exhibited linear oxidation behavior at a much smaller value than the porous alumina samples. The oxidation rates from the control samples were subtracted from the oxidation rates observed from the porous alumina samples, resulting in a value of the oxidation rate based solely on oxidation through the porous alumina overcoats (thus excluding contributions through the porous alumina cement).

## **RESULTS AND DISCUSSION**

---

### **COUNTER-CURRENT GASEOUS DIFFUSION MODEL**

The incompatibility between  $O_2$  and CO gases results in two separate regions within the porous layer. Near the graphite, the gaseous species present are CO,  $CO_2$  and  $N_2$ . In the outer region of the porous layer, the gaseous species present are  $O_2$ ,  $CO_2$  and  $N_2$ . Between these two regions, a "flame front" exists within the pores at which  $O_2$  and CO react to form  $CO_2$ :



This reaction is a sink for gas molecules, which results in net gas flow, from both regions, towards the flame front. On either side of the flame front, CO and CO<sub>2</sub> counter-diffuse and CO<sub>2</sub> and O<sub>2</sub> counter-diffuse as shown in Fig. 2. The reaction at the graphite/porous alumina interface is:



The model assumes that the rate-limiting process is gaseous diffusion, thus there is a reaction probability of one (every CO<sub>2</sub> molecule which strikes the carbon surface reacts and there is no rate constant). The overall reaction is:

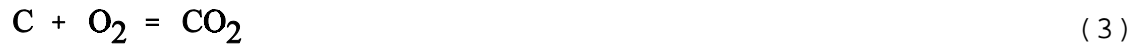


Figure 2 shows the fluxes  $J_i$  across both regions in terms of a general unit flux "a" (mol/cm<sup>2</sup>sec). The flux of each species is expressed in multiples of a (1a, 2a, etc.). The net flux of oxygen atoms inward is zero, as required by Eqs. (2) and (3).

An approximation of the Stefan-Maxwell equation<sup>6</sup> is used to calculate the gaseous concentration ( $C_i$ ) profiles across both regions of the porous alumina:

$$J_i = - D_{ieff} \left( \frac{dC_i}{dx} \right) + \left( \frac{C_i}{P/RT} \right) \sum_{j=1}^n J_j \quad (4)$$

in which  $D_{i\text{eff}}$  is an effective diffusion coefficient of gas species  $i$ , and  $x$  is the distance from the graphite/porous alumina interface. Equation (4) contains both a diffusive term and a "wind" or convective term--due to the production or destruction of gas molecules. The wind term is necessary due to the gas molecule sink at the flame front. The solutions to Eq. (4) at any position  $x$  in the graphite-side of the flame front are:

$$C_{CO} = \left( C_{CO}^* - 2c \right) e^{\left( \frac{a(x-\lambda)}{cD_{CO\text{eff}}} \right)} + 2c \quad (5)$$

$$C_{CO_2} = \left( C_{CO_2}^* + c \right) e^{\left( \frac{a(x-\lambda)}{cD_{CO_2\text{eff}}} \right)} - c \quad (6)$$

$$C_{N_2} = C_{N_2}^* e^{\left( \frac{a(x-\lambda)}{cD_{N_2\text{eff}}} \right)} \quad (7)$$

$$C_{O_2} = C_{O_2}^\circ + \frac{a(x-L)}{D_{O_2\text{eff}}} \quad (8)$$

The solutions to Eq. (4) on the gas-side of the flame front are:

$$C_{CO_2} = C_{CO_2}^\circ + \frac{a(L-x)}{D_{CO_2\text{eff}}} \quad (9)$$



$$C_{N_2} = C_{N_2}^{\circ} \quad (10)$$

in which  $C_i$  has units of mol/cm<sup>3</sup>,  $\lambda$  is the distance from the graphite/porous alumina interface to the flame front,  $L$  is the distance from the graphite/porous alumina interface to the outer edge of the porous alumina,  $c$  is the molar concentration of gas ( $P/RT$ ),  $C_i^*$  is the value of  $C_i$  at  $x$  equal to  $\lambda$ , and  $C_i^{\circ}$  is the value of  $C_i$  at  $x$  equal to  $L$ .

Using Eqs. (5-10), the concentrations of CO and CO<sub>2</sub> at the graphite/porous alumina interface can be shown to be equal to:

$$C_{CO} = -2ce \left( \frac{C_{O_2}^{\circ} D_{O_2eff} - aL}{cD_{COeff}} \right) + 2c \quad (11)$$

and

$$C_{CO_2} = \left( C_{CO_2}^{\circ} + \frac{C_{O_2}^{\circ} D_{O_2eff}}{D_{CO_2eff}} + c \right) e \left( \frac{C_{O_2}^{\circ} D_{O_2eff} - aL}{cD_{CO_2eff}} \right) - c \quad (12)$$

Equations (11-12) are used to calculate the gas compositions by finding the value of the flux,  $a$ , for which the ratio  $C_{CO}^2/C_{CO_2}$  at

the graphite/porous alumina interface is the same as the equilibrium constant of Eq. (2).

In Eqs. (11-12) the flux and porous alumina thickness are always found together as the product  $aL$ , which has units of permeability. The product  $aL$  is constant and is independent of time. The oxidation rate is proportional to the flux, "a", and thus the oxidation rate is proportional to  $1/L$ .

The above equations utilize an effective diffusion coefficient  $D_{ieff}$ . For diffusion in porous oxides, an effective diffusion coefficient is needed that decreases the overall flux of gas due to the effects of porosity, tortuosity and gas molecule interactions with pore walls. For gas species  $i$  these effects introduce an effective molecular diffusion coefficient  $D_{Mieff}$  and an effective Knudsen diffusion coefficient  $D_{Kieff}$ , which are related to  $D_{ieff}$  by<sup>6</sup>:

$$D_{ieff} = \frac{1}{(1 - \alpha N_i)/D_{Mieff} + 1/D_{Kieff}} \quad (13)$$

where  $N_i$  is the mole fraction of  $i$  and  $\alpha$  is equal to:

$$\alpha = 1 - (M_i/M_{N_2})^{1/2} \quad (14)$$

and where  $M_i$  is the molecular weight of  $i$ . The effective Knudsen diffusion coefficient can be expressed by<sup>6</sup>:

$$D_{Kieff} = (4/3)\mu_1 K \quad (15)$$

where  $\mu$  is the molecular velocity of  $i$  and  $K$  is the Knudsen permeability. Evans, Watson, and Mason<sup>7</sup> have shown that for a capillary,  $K$  is equal to one half of the average pore radius  $r$ . This is used as the estimate of  $K$  for determining  $D_{ieff}$ . The effective molecular diffusion coefficient is usually expressed as:

$$D_{Mieff} = (\phi/\tau)D_{im} \quad (16)$$

where  $\phi$  is the fractional porosity,  $\tau$  is the tortuosity, and  $D_{im}$  is an effective binary diffusivity in a multicomponent system<sup>6</sup>. Kim, Ochoa, and Whitaker<sup>8</sup> have determined that:

$$\tau = \phi^{-0.4} \quad (17)$$

gives a good empirical fit for relating porosity to tortuosity for porosities less than 50%. It has been shown that  $D_{im}$  can be found by combining Eq. (4) with the Stefan-Maxwell equation<sup>6</sup>:

$$\frac{\partial C_i}{\partial x} = \frac{n}{\sum_{j=1}^n} \frac{1}{D_{ij}} (N_i J_j - N_j J_i) \quad (18)$$

in which the binary interdiffusion coefficient  $D_{ij}$  is expressed by using the Lennard-Jones 6-12 potential:

$$D_{ij}(cm^2/sec) = 1.8583 \times 10^{-3} \frac{T^{3/2}}{P\sigma^2\Omega} \left( \frac{1}{M_i} + \frac{1}{M_j} \right)^{1/2} \quad (19)$$

where  $\sigma$  is the collision diameter in angstroms and  $\Omega$  is the collision integral.

When Eqs. (13-19) are applied to the calculation of the concentration profiles, an average value of  $N_i$  is used in Eq. (18) for each gas specie on both sides of the flame front. Iterative calculations are used to ensure self-consistency between the related concentration profiles and effective diffusion coefficients.

Examples of the diffusion coefficients found in these calculations are given in Table 2. The effects of porosity, tortuosity, and interactions with pore walls decrease the diffusion coefficient by a factor of five to eight.

Figure 2 shows the calculated gas concentration profiles, from Eqs. (5-10), in terms of partial pressures, across both sides of the flame front at a temperature of 800°C. The curves on the graphite-side of the flame front for the partial pressures of each gas specie look linear in Fig. 2, even though Eqs (5-7) are non-linear. However, the curves for CO and N<sub>2</sub> in fact have a very slight positive inflection and the curve for CO<sub>2</sub> has a very slight negative inflection (on the graphite-side of the flame front).

Below 800°C, the equilibrium constant of Eq. (2) changes rapidly to a much lower value, which shifts the relative position of the flame front closer to the graphite/alumina interface. The shift in the flame front below 800°C decreases the slopes of the gaseous species concentrations, which decreases the diffusion of gaseous species and thus decreases the oxidation rate.

## EXPERIMENTAL RESULTS

Experimental data of oxidation of graphite through porous alumina consist of mass measurements as a function of time. A representative experiment is shown in Fig. 3 for the case of a P-6-C alumina overcoat at 773°C in terms of mass change per unit area verses time. The resulting curves are linear, and the slope is the overall oxidation rate. This experiment was run in sequence with  $P_{O_2}$ 's of 0.044, 0.199, 0.50, and 0.044. The closeness in slopes between the first and last portions of the experiment (where  $P_{O_2} = 0.044$ ) shown in Fig. 3 indicate that no cracking or substantial geometric changes took place during the experiment.

Similar results are found (at lower mass losses) for control experiments using a dense alumina overcoat instead of a porous alumina overcoat. The mass loss in the control experiments is from porosity in the alumina cement used to attach the sample pieces together. For a given temperature and  $P_{O_2}$ , the oxidation rate through the porous alumina overcoat is the difference between the overall oxidation rate and the control oxidation rate. Because of sample-to-sample variations in the application of the alumina cement, control oxidation rates showed a significant amount of scatter. At each  $P_{O_2}$ , linear regression was used to fit the data in terms of oxidation rate versus  $1/T$ . Because the control oxidation rates were one to two orders of magnitude

lower than the overall oxidation rates, the scatter in the control data was not considered to be significant.

The remainder of the experimental results will be presented in the following section, shown only in terms of oxidation rates through the porous alumina overcoats.

## **COMPARISON OF THE MODEL WITH EXPERIMENTAL RESULTS**

### Oxygen Partial Pressure:

The gaseous counter-current diffusion model was used as a comparison to the experimental results. The model uses the porous alumina characteristics found in Table 1, and the temperature and  $P_{O_2}$  conditions used in the experiments. There are no adjustable parameters and there is no "fitting" of the data. The results are shown in Figs. 4-8 for porous alumina overcoats of AP-998-C, P $\frac{1}{2}$ B-C, P-6-C, P-12-C, and P-40-C, respectively. The results in Fig. 4 for the overcoat of AP-998-C show a consistent overestimation by the model of the oxidation rates. The slopes of the prediction curves are also greater than in the data. The comparisons in Fig. 5 for the overcoat of P $\frac{1}{2}$ B-C are closer than for the AP-998-C overcoat--in terms of both the magnitude and slope of the predictions. In Fig. 6 for an overcoat of P-6-C, the predicted values of the oxidation rates are close to the experimental values, but the slopes of the predicted curves are somewhat higher than found experimentally. In Fig. 7 for an overcoat of P-12-C, the model's predictions are very close to the experiment, except for some of the low temperature (570°C)

experiments. The model's predictions for overcoat P-40-C in Fig. 8 are consistently low at 670°C and above, but the slopes are quite close between the predictions and experimental data.

While there is not total agreement between the experimental data and the predictions of the model, the overall comparison is a favorable one, especially considering the approximations used for estimating  $D_{ieff}$  through the porous alumina overcoat.

#### Porosity and Average Pore Radius:

The relationship between porosity, average pore radius, and oxidation rate is illustrated in Fig. 9, which shows a family of curves having different oxidation rates. The curvature is a result of Eq. (13), and separates the graph into three regimes: where Knudsen type diffusion dominates, where viscous flow dominates, and a mixed regime where both contribute. The range of porosities and average pore radii in the five alumina overcoats span the transition between diffusion controlled by molecular diffusion and Knudsen diffusion. A direct comparison between the oxidation rates through each of the overcoats to examine the role of porosity and average pore radius is not meaningful due to differences in thicknesses between the overcoats. However, as was shown, a prediction of the model is that the oxidation rate is proportional to the reciprocal of the overcoat thickness. Thus for comparison in Fig. 9, the oxidation rates through the various porous overcoats were normalized to the same thickness, *i.e.*, 0.65 cm. The differences between experiment and model predictions in Fig. 9 are the same as in Figs. 4-8 at 770°C. The

most favorable comparisons at 770°C and  $P_{O_2} = 0.199$  in Fig. 9 are for the P-6-C and P-12-C overcoats. As indicated in Table 2, the mercury porosimeter measurements for P-12-C and P-40-C revealed a bimodal distribution in average pore radius. The presence of the bimodal distribution appears to neither help or hinder the comparisons between experiment and the model for the P-40-C or P-12-C overcoats.

#### Temperature:

The relationship between the oxidation rate and reciprocal temperature is shown in Fig. 10 for oxidation through P-12-C with a  $P_{O_2}$  of 0.199. The slope is proportional (with a negative coefficient) to the apparent activation energy. The apparent activation energies predicted by the model range from 2.2 kJ/mol at 400°C to 9.6 kJ/mol at 620°C to 2.9 at 1100°C, which are in the range one would expect for a gaseous diffusion controlled mechanism. One should note that while Fig. 10 extends down to 400°C, it is expected that reaction controlled kinetics would replace diffusion controlled kinetics at some point.

The position of the flame front as a function of temperature is also displayed in Fig. 10. As the temperature decreases from about 800°C, the flame front shifts from the middle of the porous overcoat closer and closer to the graphite/alumina interface. This shift is due to changes in the equilibrium constant of Eq. (2). The apparent activation energy is highest over the temperature range where the flame front shifts the most. The experimental data points in Fig. 10 have too much scatter to resolve any



shifts in the apparent activation energy with changes in temperature.

#### **APPLICATION OF THE MODEL TO OTHER OXIDATION SYSTEMS**

The counter-current gaseous diffusion model was first developed for the oxidation of HfC<sup>1-4</sup> and is presented here for the oxidation of graphite through porous alumina overcoats. Any system with gaseous oxidation products and a porous or cracked scale or coating is a candidate for the oxidation being controlled by counter-current gaseous diffusion. One example would be the oxidation of other metal carbide systems, such as ZrC. Another example would be high temperature coating systems in which a porous oxide overcoat is applied to help resist erosion oxidation, to immobilize a protective glass film, or to serve as a thick stagnant boundary layer. The model has also been postulated to describe the oxidation of carbon-carbon composites through a cracked SiC coating during cooling from elevated temperatures<sup>1</sup>.

In the Bernstein and Koger<sup>5</sup> model for carbon film undercut kinetics, one of the boundary conditions was pure CO gas at the carbon interface, rather than using an equilibrium constant to relate the CO and CO<sub>2</sub> partial pressures. This results in a constant flame front position (no shift), and therefore no strong temperature dependence is predicted. Yet below 700°C, the measured oxidation rates were found to be slower than expected, as would be predicted by a shift in the flame front. Jacobson

and Rapp<sup>9</sup> used a similar gaseous diffusion model for describing the oxidation of a carbon/carbon composite beneath a SiC coating containing pinholes. Due to the high temperatures involved (1200-1700°C), the estimate of a very small CO<sub>2</sub> partial pressure at the carbon/carbon composite surface was good--no shift in the position of the flame front is expected at these temperatures.

Another application is the oxidation of carbon within carbon fiber reinforced ceramic matrix composites. In the case of carbon fibers in a SiC matrix, the critical temperature regime (for carbon oxidation) is 600 to 1000°C<sup>10</sup>. Below 600°C, the whole system is stable. Above 1000°C, the SiC matrix tends to be self-healing. Cawley, Ünal, and Eckel<sup>10</sup> discuss important aspects of gas-phase diffusion controlled kinetics (parabolic) versus chemical reaction controlled kinetics (linear). Filipuzzi and Naslain<sup>11</sup> present a model that incorporates pore-size changes during the oxidation process--to predict healing by SiC oxidation. Neither of these studies incorporate a flame front within the pore.

#### **CHEMICAL VAPOR INFILTRATION**

Another candidate system for applying the counter-current gaseous diffusion model is chemical vapor infiltration (CVI). CVI is a type of chemical vapor deposition (CVD) in which gaseous reactants diffuse into a porous substrate, react and deposit on the substrate, as gaseous products diffuse outward. A limitation of CVI is that the reactants and gaseous products have to diffuse

in and out through long and possibly tortuous channels--without depositing and choking off the channels. To avoid choking off the channels, the overall kinetics have to be controlled by surface reaction kinetics--not gaseous diffusion. Thus, low temperatures and pressures are needed, which necessitate long densification times<sup>12</sup>. So in CVI processes, it is desirable to operate at the highest temperature for which the kinetics are surface reaction controlled--in order to speed up the process. A modified counter-current gaseous diffusion model would be an aid in modeling diffusion kinetics for comparison with surface reaction kinetics for determining optimal operating temperatures. The major modification in the model would be to allow for changes in the porosity and pore size with time, to simulate pores closing up. The efforts of Filipuzzi and Naslain<sup>11</sup> could perhaps form the basis for such a modification.

CVI in the presence of a thermal gradient can achieve greater densities. The gaseous reactants diffuse from the cold side and deposit on the hot side<sup>12</sup>. The diffusion equations used in the model could be expanded to include temperature gradients.

These changes would increase the complexity of the model considerably. Another improvement for CVI applications of the model would be to account for the possible anisotropic nature of the substrate and its effects on the effective diffusion coefficients, perhaps as described by Kim, Ochoa, and Whitaker<sup>8</sup>.

#### SUMMARY AND CONCLUSIONS

---

A counter-current gaseous diffusion model was developed for describing the oxidation of graphite through porous alumina overcoats. The model separates the porous alumina into two gas diffusion regions separated by a flame front, where  $O_2$  and CO react to form  $CO_2$ . In the outer region (air-side)  $O_2$  and  $CO_2$  counter-diffuse; in the inner region (graphite-side)  $CO_2$  and CO counter-diffuse. The simplified form of the Stefan-Maxwell equation, coupled with the effects of porosity, tortuosity, and gas-wall interactions are introduced. The concentration gradients of each gaseous specie in the pores of the alumina are determined and the rate of oxidation is calculated. It was shown that the oxidation kinetics are proportional to the reciprocal of the alumina thickness.

Experimental verification of the model could not prove conclusively that the counter-current diffusion model was absolutely correct. Scatter in the data and uncertainties in calculating  $D_{i\text{eff}}$  were too great. However, the model (without any adjustable parameters) was shown to have good predictive results in terms of overall oxidation rate values and how oxidation rates vary with  $P_{O_2}$ , temperature, porosity, and average pore radius.

Applications of the model to other systems are possible in systems with a gaseous oxidation product and a porous or cracked coating or scale. Other candidate oxidation applications include the oxidation of metal carbides such as HfC and ZrC, the oxidation through porous oxide overcoats in high-temperature coating systems, the oxidation of carbon (or carbon-carbon composites)

through cracks or pores in a scale, and the oxidation of carbon reinforced ceramic matrix composites. Additionally, for carbon film undercut oxidation kinetics used for describing the fabrication of micromechanical structures<sup>5</sup>, it was shown that the present model should provide a better description of the low temperature kinetics. The possible use of the counter-current gaseous diffusion model was also described for CVI.

#### REFERENCES

---

1. G.R. Holcomb, "The High Temperature Oxidation of Hafnium Carbide" (Ph.D. diss., The Ohio State University, 1988).
2. J.T. Prater, "Modification of Hafnium Carbide for Enhanced Oxidation Resistance Through Additions of Tantalum and Praseodymium," Air Force Report, AFWAL-TR-88-4141, 1988.
3. E.L. Courtright, J.T. Prater, G.R. Holcomb, G.R. St. Pierre, R.A. Rapp, *Oxidation of Metals* 36, 5/6 (1991): p. 423.
4. G.R. Holcomb, G.R. St. Pierre, *Oxidation of Metals* 40, 1/2 (1993): p. 109.
5. J. Bernstein, T.B. Koger, *J. Electrochem. Soc.* 135, 8 (1988): p. 2086.
6. K. Schwerdtfeger, E.T. Turkdogan, "Equilibria and Transport Phenomena Involving Gas Mixtures and Condensed Phases," in *Physicochemical Measurements in Metals Research*, ed. R.A. Rapp (New York, NY: John Wiley and Sons, 1970), p. 321.
7. R.B. Evans, G.M. Watson, E.A. Mason, *J. Chem. Phys.* 35 (1961): p. 2076.

8. J.H. Kim, J.A. Ochoa, S. Whitaker, *Transport in Porous Media* 2 (1987): p. 327.
9. N.S. Jacobson, R.A. Rapp, "Thermochemical Degradation Mechanisms for the Reinforced Carbon/Carbon Panels on the Space Shuttle," NASA Technical Memorandum, 106793, January, 1995.
10. J.D. Cawley, Ö. Ünal, "Oxidation of Carbon in Continuous Fiber Reinforced Ceramic Matrix Composites," in *Ceramic Transactions: Advances in Ceramic Matrix Composites*, Vol. 38, ed. by N.P. Bansal (Westerville, OH: American Ceramic Society, 1994), pp. 541-552.
11. L. Filipuzzi, R. Naslain, *J. Am. Ceram. Soc.* 77, 2 (1994): pp. 467-480.
12. H.O. Pierson, *Handbook of Chemical Vapor Deposition (CVD): Principles, Technology, and Applications* (Park Ridge, NJ: Noyes Publications, 1992), p. 116.

Table 1. Results of Mercury Porosimeter Measurements and Thickness of the Porous Coors Aluminas.

Alumina	Porosity	Average Pore Radius ( $\mu\text{m}$ )	Alumina Thickness (cm)
AP-998-C	0.25	0.160	0.27
P $\frac{1}{2}$ B-C	0.39	0.077	0.62
P-6-C	0.36	0.831	0.62
P-12-C	0.44	1.93 <sup>A</sup>	0.65
P-40-C	0.34	10.04 <sup>B</sup>	0.63

<sup>A</sup>A bimodal distribution with peaks at about 1 and 4  $\mu\text{m}$ .

<sup>B</sup>A Bimodal distribution with peaks at about 0.5 and 12  $\mu\text{m}$ .

Table 2. Calculated Diffusion Coefficients at 800°C in air within Porous Alumina Overcoats P-6-C and P<sup>1</sup>/<sub>2</sub>B-C.

Species	Side of Flame Front	P-6-C		P <sup>1</sup> / <sub>2</sub> B-C	
		D <sub>im</sub>	D <sub>ieff</sub>	D <sub>im</sub>	D <sub>ieff</sub>
		(cm <sup>2</sup> /sec)	(cm <sup>2</sup> /sec)	(cm <sup>2</sup> /sec)	(cm <sup>2</sup> /sec)
CO	Graphite	1.69	0.371	1.69	0.215
CO <sub>2</sub>	Graphite	1.40	0.297	1.40	0.172
N <sub>2</sub>	Graphite	1.64	0.361	1.64	0.212
O <sub>2</sub>	Air	1.70	0.368	1.70	0.208
CO <sub>2</sub>	Air	1.40	0.297	1.40	0.172
N <sub>2</sub>	Air	1.58	0.348	1.58	0.208



## FIGURE CAPTIONS

---

- Fig. 1. Schematic of the graphite/porous alumina sample assembly.
- Fig. 2. Fluxes, reactions, and partial pressures of  $O_2$ ,  $CO$ ,  $CO_2$ , and  $N_2$  across porous alumina overcoat P-6-C during the oxidation of graphite with a  $P_{O_2}$  of 0.21 at  $800^\circ C$ . The overall reaction is  $C + O_2 = CO_2$ .
- Fig. 3. Mass change as a function of time during oxidation of graphite through porous alumina overcoat P-6-C at  $773^\circ C$ . The sample was exposed to dry  $O_2$ - $N_2$  mixtures with  $P_{O_2}$ 's (in order of exposure) of 0.044, 0.199, 0.50, and 0.044.
- Fig. 4. Experimental data (points) and predictions of the gaseous counter-current diffusion model (lines) for oxidation rates of graphite through porous alumina overcoat AP-998-C at five temperatures.
- Fig. 5. Experimental data (points) and predictions of the gaseous counter-current diffusion model (lines) for oxidation rates of graphite through porous alumina overcoat P $\frac{1}{2}$ B-C at five temperatures.
- Fig. 6. Experimental data (points) and predictions of the gaseous counter-current diffusion model (lines) for oxidation rates of graphite through porous alumina overcoat P-6-C at five temperatures.

- Fig. 7. Experimental data (points) and predictions of the gaseous counter-current diffusion model (lines) for oxidation rates of graphite through porous alumina overcoat P-12-C at five temperatures.
- Fig. 8. Experimental data (points) and predictions of the gaseous counter-current diffusion model (lines) for oxidation rates of graphite through porous alumina overcoat P-40-C at five temperatures.
- Fig. 9. Oxidation rates ( $\text{mg}/\text{cm}^2/\text{sec}$ ) as a function of porosity and average pore radius for the oxidation of graphite through porous alumina at  $770^\circ\text{C}$  with an oxygen partial pressure of 0.199. The lines, at four specific oxidation rates, were generated from the model. The open squares are normalized experimental data. The bimodal distributions in pore radius for P-40-C and P-6-C are indicated.
- Fig. 10. Oxidation rates from experiment (points) and predicted from the model (line) on the left-hand scale, and the position of the flame front,  $\lambda$ , on right-hand scale versus reciprocal temperature for oxidation of graphite through a porous P-12-C alumina overcoat at an oxygen partial pressure of 0.199.